POLITECNICO DI TORINO
Repository ISTITUZIONALE

A Method to Determine PWM-Induced High-Frequency Harmonic Losses in a Converter-Fed Induction Motor by Experimental Tests

Original
A Method to Determine PWM-Induced High-Frequency Harmonic Losses in a Converter-Fed Induction Motor by Experimental Tests / Tiihonen, M., Ahmed, S., Kärkkäinen, H., Niemelä, M., Aarniovuori, L., Nerg, J., Liu, D., Boglietti, A., Bojoi, R.. - In: IET ELECTRIC POWER APPLICATIONS. - ISSN 1751-8660. - ELETTRONICO. - 20:1(2026), pp. 1-11.

Availability:
This version is available at: 11583/3015827 since: 2026-09-23T06:17:00Z

Publisher:
wiley

Published
DOI:

Terms of use:

This article is made available under terms and conditions as specified in the corresponding bibliographic description in the repository

Publisher copyright

(Article begins on next page)

21 November 2026

Check for updates

IET Electric Power Applications

WILEY

The Institution of Engineering and Technology

ORIGINAL RESEARCH OPEN ACCESS

A Method to Determine PWM-Induced High-Frequency Harmonic Losses in a Converter-Fed Induction Motor by Experimental Tests

Matias Tiihonen[1] | Shoaib Ahmed[1] | Hannu Kärkkäinen[1] | Markku Niemelä[1] | Lassi Aarniovuori[1] | Janne Nerg[1] | Dong Liu[2] | Aldo Boglietti[3] | Radu Bojoi[3]

[1]Laboratory of Electrical Drives Technology, LUT University, Lappeenranta, Finland | [2]Laboratory of Electrical Drives Technology, LUT University, Lahti, Finland | [3]Department of Energy, Polytechnic University of Turin, Turin, Italy

Correspondence: Matias Tiihonen (matias.tiihonen@lut.fi)

Received: 4 June 2026 | **Revised:** 17 August 2026 | **Accepted:** 7 September 2026

Keywords: AC machines | frequency-domain analysis | harmonics | loss measurement | pulse width modulation | standards

ABSTRACT

The additional high-frequency losses present in converter-fed machines can constitute a significant portion of the overall motor system losses. Until now, no universally accepted method has existed to quantify and analyse these losses. This paper presents a universal method for determining the additional losses caused by pulse width modulation (PWM), which is validated using an induction motor. The proposed approach for segregating high-frequency harmonic losses assumes that these losses are equivalent to the total harmonic power observed at the motor terminals. The method requires no special arrangements or instrumentation; however, its accuracy naturally depends on the quality of the measurement instruments used. Moreover, this approach adds value to the evaluation of results obtained through the commonly used input–output method for efficiency determination. The ability to explicitly determine high-frequency harmonic losses in converter-fed machines opens new opportunities for innovation in motor control systems, modulation strategies and methods for minimising losses in such systems.

1 | Introduction

Electrical motors consume almost 50% of the electrical energy produced globally [1], and the proportion of the energy consumption of electric motors is expected to increase, for example, due to the electrification of transportation [2]. The most common type of industrial motor is an induction motor (IM), which has been estimated to consume about one-third of the energy used in industrialised countries [3].

Different methods have been presented in the literature to experimentally determine loss components of direct-on-line (DOL) IMs, and standardised methods have been published for this purpose, such as in the IEEE 112 standard since 1964 [4] and later in IEC 60034-2-1 [5]. Policies and regulations have driven the continuous improvement in the efficiency of industrial motors, and finally in 2020, converter-fed motors also received their own international energy efficiency standard, IEC 60034-2-3 [6]. Before the publication of ref. [6], the applicability of the loss segregation method presented in ref. [5] was tested with converter-driven motors in ref. [7]. The standard IEC 60034-30-1 [8] defines efficiency classes for single-speed AC motors, which IMs are generally designed to be, whereas the technical specification IEC TS 60034-30-2 [9] applies to variable-speed AC motors.

Converters, which are employed to drive AC motors, use pulse width modulation (PWM) methods to provide the desired voltage level and frequency for the motor. The PWM supply produces nonsinusoidal voltage to the motor, because it outputs voltage pulses. This causes harmonics in the motor input, which

This is an open access article under the terms of the Creative Commons Attribution-NonCommercial License, which permits use, distribution and reproduction in any medium, provided the original work is properly cited and is not used for commercial purposes.

© 2026 The Author(s). *IET Electric Power Applications* published by John Wiley & Sons Ltd on behalf of The Institution of Engineering and Technology.

leads to an increase in some loss components of the motor, most significantly in the iron losses [10, 11]. The sum of the increased parts of the motor loss components can be considered as an individual loss component, which can be referred to as an additional high-frequency harmonic (HFH) loss caused by the converter supply. The amount of HFH losses in the motor is affected by the speed, input voltage, input current, design and size of the motor [12]. The amount of HFH losses are also influenced by the type and parameters of the converter through the pattern of pulses. The main system parameters that affect HFH losses are DC-link voltage, switching frequency and inductance of the driven machine. The HFH losses cause additional heating of the motor, which limits the amount of load that the motor can handle continuously in terms of cooling [13].

When driving motors with converters of the common two-level voltage source inverter (VSI) type, the HFH losses typically vary between 10% and 30% of the total losses of the motor according to the recently updated application guide IEC TS 60034-25 [12]. The loss level is significant, and thus can't be neglected from the loss analysis. The HFH losses are significant at light-load operation due to their relatively constant nature. However, the accurate determination of the losses is a prerequisite for their effective and reliable analysis, and this remains a challenge to this day. Different approaches, such as modelling and experimental testing have been proposed.

Various finite element (FE) approaches have been implemented to model the HFH losses. In ref. [14], the FE method was used to model PWM-induced additional core losses by tuning the model with measurement data. In ref. [15], the FE method was used for modelling the core, stray-load and harmonic core losses of IMs with different electrical steels installed in them. The most accurate results can be obtained by using the time-stepping FE method with a small calculation time step [16, 17]; however, the method is extremely time consuming. A faster method was proposed in ref. [18]; the approach uses both time-varying and spatial information of the electromagnetic quantities. Typically, loss models are not incorporated in the FE method solution, but they are part of the postprocessing procedure to obtain the losses. The electromagnetic losses of a 5.5 kW IM were analysed in ref. [19], taking into account the interbar current and rotor slip frequency. The coupling between the time and space harmonics was considered by using a two-term piecewise-defined variable coefficient iron loss model together with finite element analysis (FEA). A comprehensive mathematical core loss model for a PWM-supplied induction motor was presented in ref. [20]; the model can be used together with FEA. The model includes the losses produced by fundamental and inverter harmonics, surface losses caused by saturation harmonics, tooth pulsation harmonic losses and additional core losses due to leakage flux. In addition to FE approaches, a method to determine the additional HFH losses based on harmonic regression analysis is presented in ref. [21].

In this paper, an experimental method for determining the additional HFH losses for converter-fed induction motors is proposed and verified. The method should also be applicable to other types of AC motors, but here the focus is only on IMs. The method is based on performing a frequency domain analysis (FDA) with measured voltage and current waveform data to differentiate phenomena at different frequencies from each other and to form a power spectrum as a function of frequency. The power spectrum is used to determine the input power at the fundamental wave frequency, which is the supply frequency of the motor.

The FDA method applied in this paper has been used in refs. [22–24] and recently in ref. [25]. FDA has been used with motors for a long time. For example, it was used in ref. [26] to compare the performances of different modulation techniques. In part because of the limitations of computational power, partial data sets have been used before. This has led to the loss of information in the process. Here, the data sets are long enough and recorded with a high sampling rate, so that the power is the same regardless of whether it is calculated in the frequency domain or in the time domain. FDA also allows the extraction of the fundamental voltage and current values from the measured data. Using these extracted values, the fundamental proportions of the motor loss components can be determined, and therefore, this approach is used in this paper to verify the proposed HFH loss determination method.

2 | Determination of the PWM-Induced High-Frequency Harmonic Losses Experimentally

To date, all widely adopted methods for harmonic loss determination have been based on a comparison between converter supply and sinusoidal supply. Two of these standard methods described below are performed without full load at the desired point.

In the standard IEC 60034-2-3 [6], a loss summation method is presented for determining different loss components of the converter-fed induction motor. The method can be used to determine the amount of additional losses, which are present only in the converter-fed motor, in an indirect way. A method defined in an older technical specification, IEC TS 60034-2-3 [27], which was replaced by the standard, is more complicated but takes into account the effect of the motor load level on the HFH losses. The standard [6] also presents a direct input–output method to determine the efficiency of a converter-fed motor. However, this method does not provide a way to determine the additional HFH loss component.

2.1 | Indirect Standard Method

In IEC 60034-2-3 [6], the HFH losses are determined by running a single test point at no-load with both the converter supply and the sinusoidal supply. The HFH losses are then calculated as the difference of the constant losses

$$P_{\mathrm{HFH}} = P_{\mathrm{c,con}} - P_{\mathrm{c,gen}}, \tag{1}$$

where $P_{\mathrm{c,con}}$ is the constant loss value with the converter supply, and $P_{\mathrm{c,gen}}$ is the constant loss value with the sinusoidal supply. The constant losses are the difference between the no-load electric input power and the no-load stator losses. In the standard, the HFH losses are considered to be independent of the motor load level.

17518679, 2026, 1, Downloaded from https://ietresearch.onlinelibrary.wiley.com/doi/10.1049/elp2.70232 by Politecnico Di Torino Sist. Bibl Del Polit Di Torino, Wiley Online Library on [12/11/2026]. See the Terms and Conditions (https://onlinelibrary.wiley.com/terms-and-conditions) on Wiley Online Library for rules of use; OA articles are governed by the applicable Creative Commons License

2.2 | Indirect Technical Specification Method

A method presented in the IEC technical specification is mostly the same as the standard method above. However, in this method, more tests than only the no-load test are performed with the converter-fed motor. In this method, the load dependence of HFH losses is taken into account as the standard load curve test is performed for both the sinusoidal supply and the converter supply. The load-dependent proportion of the HFH losses is determined by subtracting the residual losses in the sinusoidal supply from the residual losses in the converter supply [27]. This remainder is summed up with the difference in the constant loss-based value determined with Equation (1) to get the final HFH loss value.

3 | Method Proposed in This Paper

In this section, the proposed method for determining the HFH losses of a converter-fed IM is described. In Figure 1, the steps for performing the method have been presented in a flowchart. The method is based on the following key points:

1. Raw waveform data of input voltages and currents of the three-phase motor are recorded with a power analyser for FDA.
2. Using FDA, fundamental frequency values of voltages, currents and three-phase active power are extracted.
3. The HFH loss is determined as the difference between the total active power and the fundamental active power, and is treated as its own loss component.

In the time domain, the voltage u and the current i are continuous quantities, and the active power P is defined as

$$P = \frac{1}{T}\int_0^T u(t)i(t)\,\mathrm{d}t, \tag{2}$$

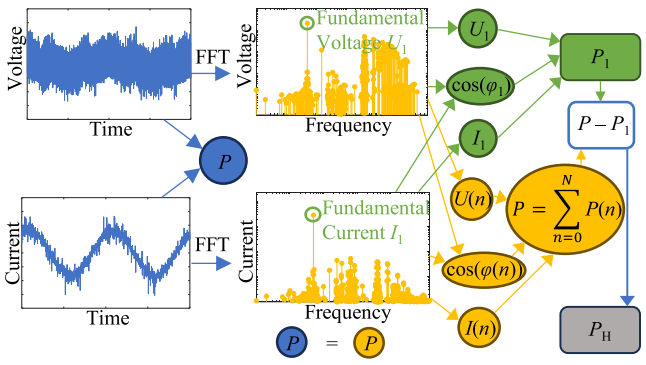


FIGURE 1 | A flow chart of the proposed method. Measurements are performed in the desired operation point with measuring both waveform data and continuous data of the electrical quantities of the motor, as well as continuous data of the mechanical quantities. Voltage and current spectra are created, fundamental voltages and currents are determined and power spectra are formed. In the figure P is the total active input power, U_1 is voltage at the fundamental wave frequency, I_1 is current at the fundamental wave frequency, $\cos(\varphi_1)$ is the power factor at the fundamental wave frequency, P_1 is the total input power at the fundamental wave frequency, and P_H is the total harmonic power of the motor.

where t is the time and T is the time of either a period or multiple periods [28]. In general, a power analyser is the most accurate device for measuring electric power. In practice, a power analyser captures the voltages and currents at a limited sampling rate for power determination, and, for example, the voltage, current and power values given by the power analyser are based on discrete time analysis. Raw waveform data with the length T recorded with a power analyser at a sampling rate S has the total number of samples

$$N = TS. \tag{3}$$

In discrete form, the active power equation becomes:

$$P = \frac{1}{N}\sum_{k=1}^{N} u(k)i(k), \tag{4}$$

where k is an index number for a sample.

For the FDA, the voltage and current waveform data must be measured with a high enough sampling frequency and waveform length for the data to be useful in the motor loss analysis. The standard 60034-2-3 [6] states that, in general, the bandwidth of 0 Hz to the switching frequency multiplied by 10 is sufficient and that automatic digital measurement equipment should take multiple samples over a time span of at least 15 s, but to a maximum of 60 s. However, these values are for total power measurements, where slower fluctuations in operation can occur. The PWM-caused phenomena are very stable in steady-state operation, and thus, the length of the waveform is only important to achieve a dense enough frequency resolution, where 1 Hz corresponding to a 1-s data length is usually enough. For the sampling rate, 1 million samples per second is generally sufficient, and thus, the total number of samples N is 1 million. These numbers are well achievable with modern power analysers with three channel voltages and currents, and also fast to analyse with typical desktop computers.

The discrete voltage and current waveform data can be converted into the frequency domain by performing discrete Fourier transform using FFT (fast Fourier transform). For an accurate fundamental frequency power calculation, rectangular windowing has to be used. In practice, this means that the waveform data length is cut to match the maximum integer number of fundamental frequency cycles. More details on signal analysis are available, for instance, in ref. [29].

With N number of samples of long waveform data, FFT yields a two-sided spectrum of complex value frequency components on both sides of the zero frequency. The two-sided spectrum has a total number of $N + 1$ components between the negative and positive Nyquist frequencies [30]. The two-sided spectrum can be converted into a single-sided amplitude spectrum with $\frac{N}{2} + 1$ components by considering only the positive side and taking the absolute value of each frequency component. In addition, as the positive side of the spectrum (nonzero frequencies) contains only half of the amplitudes, the values must be multiplied by 2 to get the actual amplitudes of each frequency component. These frequency components are amplitudes of sinusoidal signals, and thus, their RMS values are the amplitudes divided by $\sqrt{2}$. The zero frequency (DC) component has to be handled differently, as its

17518679, 2026, 1, Downloaded from https://ietresearch.onlinelibrary.wiley.com/doi/10.1049/elp2.70232 by Politecnico Di Torino Sist. Bibl Del Polit Di Torino, Wiley Online Library on [12/11/2026]. See the Terms and Conditions (https://onlinelibrary.wiley.com/terms-and-conditions) on Wiley Online Library for rules of use; OA articles are governed by the applicable Creative Commons License

(absolute) value is already the correct one (as there is only one zero component), and for DC there is no difference in terms of the amplitude or RMS values.

Fast Fourier transform is applied to all three phase voltage and current waveforms returning the complex values U and I, respectively. For power calculation, the amplitude and angle information is needed, and as mentioned above, the amplitudes of the voltage and current $\widehat{U}$ and $\widehat{I}$ are obtained as the absolute values of the complex quantities. The power factor $\cos(\varphi)$ is determined for each frequency component by calculating the phase difference φ between voltage and current, which is obtained by subtracting the phase angle of the current from the phase angle of the voltage

$$\varphi(n) = \arg(U(n)) - \arg(I(n)), \tag{5}$$

where $n = 0, 1, ..., N$ is the index of the frequency component, and $U(n)$ and $I(n)$ are the complex values of the frequency component n of voltage and current, respectively.

The active power for each sinusoidal frequency component ($n > 0$) is defined as

$$P(n) = \frac{\widehat{U}(n)}{\sqrt{2}} \frac{\widehat{I}(n)}{\sqrt{2}} \cos(\varphi(n)), \tag{6}$$

where $\widehat{U}(n)$ and $\widehat{I}(n)$ are the amplitudes of the nth frequency component of voltage and current, respectively. For the DC component ($n = 0$), the active power is

$$P(0) = U(0)I(0). \tag{7}$$

Furthermore, the total active power is the sum of all the frequency components

$$P = \sum_{n=0}^{N/2} P(n), \tag{8}$$

where $\frac{N}{2}$ is the index of the highest frequency component of the dataset that can be analysed with the sampling frequency (Nyquist frequency) used. When the analysis is performed as presented here, the total active power results are the same with very high precision regardless of whether they are determined in the time or frequency domain.

The fundamental frequency of the electrical quantities of the converter-fed motor is the supply frequency. Using Equation (6), the active input power can now be divided into the fundamental frequency active power (the first harmonic) P_1 and the harmonic active power P_H. P_1 is obtained with Equation (6) with the frequency index n as 1, and P_H, which is the sum of other frequency components [28], can be calculated by subtracting P_1 from the total active power:

$$P_H = P - P_1. \tag{9}$$

An example of power analysis in the frequency domain is illustrated in Figure 2, where the input active power results as a function of frequency are presented for a 4-pole 15 kW induction motor as cumulative power curves with both the sinusoidal and the PWM supply. The nameplate values of the motor are given in Table 1. The cumulative active power curves were obtained as the cumulative sum of active power values calculated for each frequency by using Equation (6). The three-phase voltage and current waveforms were recorded with a sampling rate of 1 million samples per second for 1 s, that is, each of the phase quantities contains 1 million discrete samples. Relatively long sample at steady-state and high sampling frequency were used to acquire multiple periods of fundamental wave, which was done to mitigate the effect of the noise in the results and to achieve the more precise resolution. The noise distorts measurement results to some degree, but because the power at the fundamental waveform frequency is significantly higher than all other power components combined, the uncertainty of fundamental waveform frequency is more meaningful from the total power measurement point of view.

The operating point in Figure 2 is the 37.5 Hz supply frequency and 100% of the rated torque with both supplies. Most of the fundamental power steps at 37.5 Hz are scaled outside the figure to better visualise the high-frequency harmonic power. Below the fundamental frequency, there is only negligible power with a

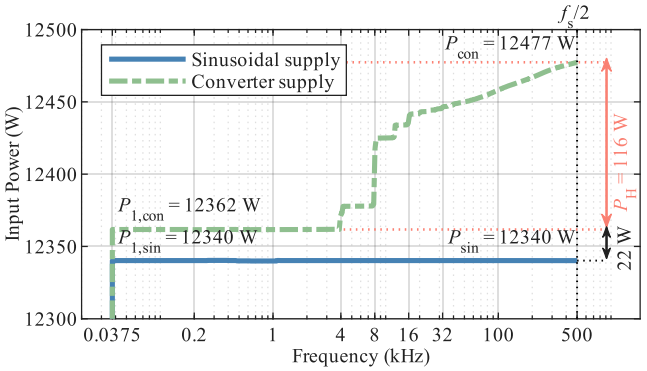


FIGURE 2 | Experimentally defined active power illustrated as cumulative power as a function of frequency, while the carrier frequency is 4 kHz. The sampling frequency f_s is 1 MHz, and thus, according to the Nyquist theorem, the highest frequency component that can be analysed is 500 kHz. Total power is calculated by using all frequency components, and thus, as the frequency components are illustrated cumulatively, the highest frequency component represents the total active power. The switching frequency f_{sw} causes frequency components at multiples of 4 kHz, such as 8 and 16 kHz. Harmonic power on frequencies lower than the fundamental wave frequency are summed in P_H but not presented in the figure.

TABLE 1 | Details of the Δ-connected motor under test.

Symbol	Variable	Value	Unit
P_n	Rated power	15	kW
n_n	Rated speed	1474	min^{-1}
U_n	Rated voltage	400	V
I_n	Rated current	27.8	A
$\cos(\varphi_n)$	Rated power factor	0.84	
f_n	Rated frequency	50	Hz
η_n	Rated efficiency	92.7	%

17518679, 2026, 1, Downloaded from https://ietresearch.onlinelibrary.wiley.com/doi/10.1049/elp2.70232 by Politecnico Di Torino Sist. Bibl Del Polit Di Torino, Wiley Online Library on [12/11/2026]. See the Terms and Conditions (https://onlinelibrary.wiley.com/terms-and-conditions) on Wiley Online Library for rules of use; OA articles are governed by the applicable Creative Commons License

cumulative value of less than 0.1 W with both supplies, and thus, no practical information is lost when scaling the vertical axis.

The curve with the generator supply (blue solid line) in Figure 2 contains power practically only at the fundamental wave frequency. The curve with the frequency converter supply (green dashed line) contains slightly more power at the fundamental wave frequency and a high amount of harmonic power at the 4, 8, 12 and 16 kHz frequencies that are formed by the carrier frequency of 4 kHz and its multiples. The difference between the total input power of the converter supply and the sinusoidal supply is 1.1%.

The results presented in Figure 2 are based on a single 1-s long waveform data recorded with a power analyser designed to investigate high-frequency phenomena, and there is a 0.17% (22 W) difference in the input power at the fundamental wave frequency. Slight differences in the fundamental power values of the waveforms are inevitable due to small fluctuations in the motor and load operation and due to the difficulty of matching the input power exactly with the generator and converter supplies in general. Some of the fundamental power difference is also due to the higher total motor losses with the converter, which causes the motor to run slightly hotter, thereby increasing the resistive fundamental losses to a small degree. Typically, numerical values, such as total losses or constant losses of the motor, are used to determine the HFH losses as a comparison of the sinusoidal supply and the converter supply. When comparing two separate measurement results with only the total values, the differences in the amplitude of the fundamental waveform cannot be determined. Therefore, this difference incorrectly ends up being included in the HFH loss value; for example, in the case of Figure 2, the HFH loss value calculated as the difference of the total power values would be 138 W, whereas a more correct value based on only the harmonic power is 116 W.

The additional high-frequency power in the converter supply is formed by the time harmonics of the PWM supply. Figure 2 shows that there is practically no harmonic power with the generator supply or the frequency converter supply below the carrier frequency of 4 kHz. Hence, if the fundamental wave frequencies of the curves are identical, the additional high-frequency harmonic power is the only difference between the curves.

Furthermore, as the high-frequency power harmonics do not produce any usable torque in AC machines [28], the harmonic active power must be consumed as losses in the motor, which leads us to the main principle behind the proposed method: based on Equation (9), the total harmonic power can be calculated by subtracting the fundamental frequency power from the total active input power. As discussed above and illustrated in Figure 2, this value represents the harmonic power with the converter supply, as the total active input power consists practically only of the fundamental frequency active power and the high-frequency active power. Therefore, this paper proposes that the HFH losses P_{HFH} of a converter-fed motor can be directly determined from electric signals as the total harmonic active input power value with Equation (9).

4 | Verification of the Proposed Method Using Laboratory Measurements

As discussed in the previous section, the proposed method for harmonic loss determination relies on the assumption that the measured harmonic active input power is equal to the amount of harmonic losses occurring in the motor. This statement requires further verification, which is provided in this paper by laboratory measurements and loss analysis of the 15 kW induction motor.

4.1 | Verification Methodology

The verification procedure is illustrated in Figure 3. Measurements with the converter supply and the sinusoidal supply are performed at 16 matching operating points, and the harmonic active power P_H and the four main motor loss components are determined for all operating points. The stator Joule losses $P_{s,1}$, the rotor Joule losses $P_{r,1}$ and the iron losses $P_{Fe,1}$ are determined using fundamental frequency voltages and currents, and the mechanical losses P_{fw} with the retardation test. When the total harmonic power and the four fundamental frequency loss components are subtracted from the total losses P_T, we obtain the leftover loss component P_{Lo} as a result. If the value of P_{Lo} is similar with the sinusoidal supply and the converter supply, the harmonic losses have to be equal to the harmonic active power, and the proposed method is valid.

In this paper, the segregation of the four main loss components is performed mostly based on the principles, tests and equations of the well-known DOL IM loss segregation methodology. The DOL IM loss segregation method is presented, for example, in the standard IEC 60034-2-1 [5]. The tests required here are a heatrun test, a no-load test and a retardation test. The heatrun test is exactly the same as the rated load test in the IEC standard method, but it is performed for any test point. The no-load test is performed at the same fundamental supply frequency as the heatrun test and only at a single voltage value, because the fundamental output voltage (or flux linkage) cannot be adjusted

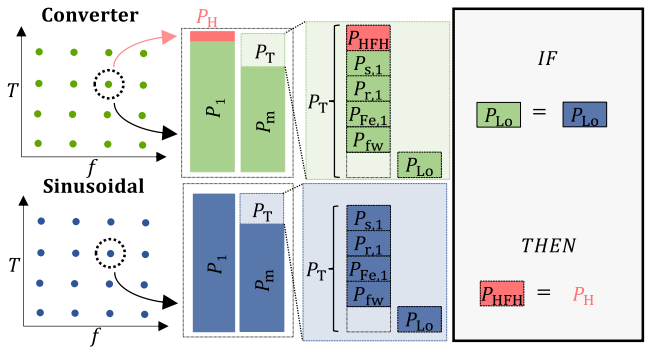


FIGURE 3 | Simplified graphical presentation of the procedure used in the verification of the proposed method. The principle of the procedure is that harmonic power P_H and fundamental power P_1 are extracted from the waveform data and fundamental loss components are determined by measured data. This is done at 16 operating points by both the sinusoidal supply and the converter supply, after which the leftover losses are compared between the supply types. If they are the same, then the HFH loss is equal to harmonic power.

17518679, 2026, 1, Downloaded from https://ietresearch.onlinelibrary.wiley.com/doi/10.1049/elp2.70232 by Politecnico Di Torino Sist. Bibl Del Polit Di Torino, Wiley Online Library on [12/11/2026]. See the Terms and Conditions (https://onlinelibrary.wiley.com/terms-and-conditions) on Wiley Online Library for rules of use; OA articles are governed by the applicable Creative Commons License

in the frequency converter, which is often the case for commercial devices. Consequently, as a single no-load test point cannot be used to determine the mechanical losses (friction and windage losses), the retardation test is used for that purpose. The retardation test method is described, for example, in IEC 60034-2-2 [31].

The mechanical losses P_{fw} are assumed to not depend on the motor supply, but only on the motor temperature, which is taken into account by performing several retardation tests at different motor temperatures. The fundamental electrical loss components $P_{\mathrm{s},1}$, $P_{\mathrm{r},1}$ and $P_{\mathrm{Fe},1}$ are assumed to correspond to the motor loss components with a purely sinusoidal supply. With this assumption, the fundamental values of the measurement data obtained using FDA can be used in the analysis to determine the fundamental motor loss components also for the converter-fed motor.

In the following, the verification methodology is described in detail to obtain the results for a single operating point, referred to as 'the test point'.

In the analysis, fundamental voltages and currents must be used, and they are accurately determined by the FDA; see Section 3. In addition, the active power has to be split into fundamental power and harmonic power, which can be done by first accurately calculating the fundamental power using the FDA and then calculating the harmonic active power using Equation (9).

In the heatrun test, the motor is run at the test point torque and speed until the rate of change of the winding temperature rise is less than 1 K in 30 min. The fundamental stator Joule losses P_{s} and the rotor Joule losses P_{r} are calculated from the results of the heatrun test. The fundamental stator Joule losses are calculated as

$$P_{\mathrm{s},1} = 1.5 R_{\mathrm{s}} I_1^2, \tag{10}$$

where I_1 is the fundamental frequency supply phase current and R_{s} is the line-to-line DC resistance of the stator windings at the heatrun test temperature. The fundamental rotor Joule losses are calculated as

$$P_{\mathrm{r},1} = \left(P_1 - P_{\mathrm{s},1} - P_{\mathrm{Fe},1}\right) s, \tag{11}$$

where P_1 is the test point fundamental input power, $P_{\mathrm{Fe},1}$ is the fundamental iron loss at no-load at the test point fundamental supply frequency, and s is the test point slip. As Equation (11) requires $P_{\mathrm{Fe},1}$, the no-load analysis has to be carried out before this calculation.

The retardation test is performed for a hot motor with the motor temperature within 5 K of the heatrun test temperature. In the retardation test, the motor is accelerated to a speed sufficiently higher than the test point speed, and the supply is cut off. After this, the motor is only rotated by the inertia of its rotating parts and decelerated by its friction and windage losses P_{fw}. Therefore, from one retardation test, P_{fw} are obtained as a function of speed for the whole retardation curve from the starting speed to the zero speed in the temperature range during the retardation test. The value of the test point P_{fw} is obtained from the retardation curve at the test point speed.

The fundamental no-load iron losses $P_{\mathrm{Fe},1}$ are determined using the single point no-load test data at the test point fundamental supply frequency, and they are calculated as

$$P_{\mathrm{Fe},1} = P_{0,1} - P_{\mathrm{s},0,1} - P_{\mathrm{fw},0}, \tag{12}$$

where $P_{0,1}$ is the no-load fundamental input power, $P_{\mathrm{s},0,1}$ are the no-load fundamental stator losses and $P_{\mathrm{fw},0}$ are the mechanical losses from the retardation test at the no-load speed and temperature. The no-load fundamental stator losses are calculated as

$$P_{\mathrm{s},0,1} = 1.5 R_{\mathrm{s},0} I_{0,1}^2, \tag{13}$$

where $I_{0,1}$ is the no-load fundamental frequency supply phase current, and $R_{\mathrm{s},0}$ is the line-to-line DC resistance of the stator windings at the no-load test temperature.

Now that all the fundamental loss components and harmonic power are known, the leftover loss term P_{Lo} can be determined. In the standard loss segregation method for DOL motors in IEC 60034-2-1 [5], residual losses are calculated by subtracting all the other loss components and the output power from the input power. Here, the leftover loss is calculated similarly with the residual losses in the DOL motor, but also the harmonic power has to be subtracted from the total input power. The leftover losses are thus calculated as

$$P_{\mathrm{Lo}} = P - P_{\mathrm{H}} - P_{\mathrm{m}} - P_{\mathrm{s},1} - P_{\mathrm{r},1} - P_{\mathrm{Fe},1} - P_{\mathrm{fw}}, \tag{14}$$

where P_{m} is the mechanical output power calculated as

$$P_{\mathrm{m}} = 2\pi n T, \tag{15}$$

where T is the test point torque, and n is the test point speed.

4.2 | Laboratory Measurements

The measurements required in the verification of the proposed method were carried out for the 4-pole 15 kW IM with nameplate values presented in Table 1. The motor is a standard totally enclosed fan cooled industrial induction machine with IEC frame size of 160. The rotor of the machine has double cage structure made from die casted aluminium and the core material is non-oriented electrical steel M400-50A. The shape and main dimensions of stator and rotor slots are presented in Figure 4 and the number of stator and rotor slots are 36/28. The frequency converter used in the tests was a commercially available VSI type frequency converter with IGBT switches. Shielded power and voltages measurement cables were used to mitigate possible high-frequency noise as demanded by the standard [6].

The focus of this paper is on the verification of the analysis method, which is the reason that a converter with widely used space-vector modulation (SVM) has been used with a 4 kHz switching frequency. Overmodulation and field-weakening were avoided for the same reason. The actual switching frequency was verified from the measured voltage waveform data

17518679, 2026, 1, Downloaded from https://ietresearch.onlinelibrary.wiley.com/doi/10.1049/elp2.70232 by Politecnico Di Torino Sist. Bibl Del Polit Di Torino, Wiley Online Library on [12/11/2026]. See the Terms and Conditions (https://onlinelibrary.wiley.com/terms-and-conditions) on Wiley Online Library for rules of use; OA articles are governed by the applicable Creative Commons License

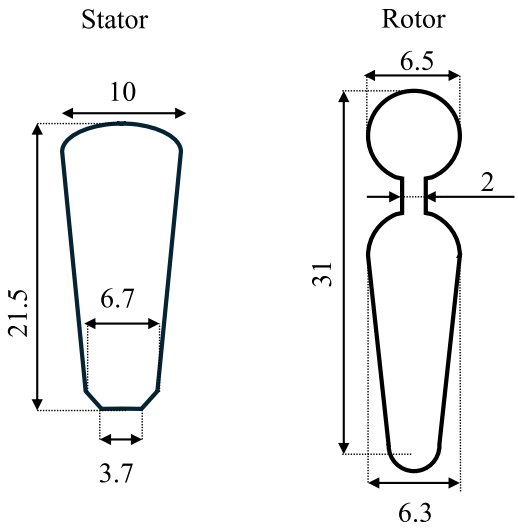


FIGURE 4 | The shape and the main dimensions of the stator and rotor slots of the motor used in laboratory measurements. The values are presented in millimetres.

by confirming that the converter did not miss any pulses, that is, that the switching frequency was indeed fixed at 4 kHz at all operating points. To avoid both overmodulation and field-weakening at 50 Hz, the frequency converter was fed with an increased input voltage from a variable transformer.

For verification of the method, the fundamental loss components at operation points measured with a sinusoidal supply were used as comparison points for the fundamental loss components at the corresponding operation points with the converter supply. For the sinusoidal supply, a fully adjustable synchronous generator was used to accurately replicate the measured fundamental frequencies and voltages of the motor driven by the frequency converter. The generator was used because the frequency fluctuations were lower than with the grid. In practice, the converter-driven motor was measured first, and measurement data was used to determine the fundamental voltage level for every measurement point. With the generator supply, the voltage level was matched in a way, that the fundamental voltage level was the same as with the converter-driven motor in the corresponding operation point. This generator supply is referred to as 'sinusoidal supply' later on.

Electrical measurement data including the voltage and current waveform data were recorded with a Yokogawa PX8000 power analyser. PX8000 is a state-of-the-art transient power analyser from Yokogawa, which has been designed to be used in high-frequency phenomena investigation and with converter-driven motor setups [32]. The bandwidth of the voltage channels in the power analyser is 20 MHz and current channels 10 MHz (−3 dB). A Hitec Zero-Flux CURACC current measurement system was used as the current transducers with 500 kHz small-signal bandwidth. A corresponding setup for obtaining electrical power was used in ref. [22], where power measurement accuracies of Yokogawa PX8000 at different frequencies were presented. A detailed description of determining measurement uncertainty for converter-fed motor setups has been presented in ref. [33]. Mechanical quantities of the motor output were obtained using an HBM T12 torque transducer with a rated torque of 100 Nm, which is very suitable in this situation because the motor has a rated torque of 97 Nm. Temperature data were obtained with a Keithley Integra Series 2701 data acquisition system with three Pt100 A-class temperature sensors attached to the stator winding of the motor. All data were recorded on a PC with a LabVIEW interface.

First, the heatrun tests were performed at 16 different operating points with the frequency converter supply. Second, the 16 heatrun tests were repeated with the sinusoidal supply matching the fundamental frequency, fundamental voltage, and load torque as accurately as possible. The torque measurement is used for matching the torque levels, when driving the motor with converter and sinusoidal supplies. The torque was fixed instead of the output power, because that way the supply frequency could also be fixed, which makes the frequency domain analysis easier. Additionally, the slip of the motor could now be used as an additional indicator for the amount of motor losses. The supply frequencies used were 12.5, 25, 37.5 and 50 Hz. The torque levels used were 25%, 50%, 75% and 100% of the rated torque of the motor. In all heatrun tests, the motor was run to thermal equilibrium before the measurement data was collected.

Next, no-load tests were performed with all the four supply frequencies with both the converter supply and the sinusoidal supply. For the no-load tests, the motor was first heated under load, then the load was decoupled, and the four supply frequencies were run in quick succession at no-load. The no-load test was repeated several times while the motor was cooling down to obtain data at the same temperatures as in the heatrun tests. This was performed at the same temperature and in the same manner with both the converter supply and the sinusoidal supply.

Lastly, retardation tests were performed. For the retardation tests, the motor was run first hot with the converter supply and then decoupled from the load. After this, the retardation test was performed by accelerating the motor to a high speed and then disconnecting the supply from the motor. The retardation test was repeated for the cooling motor until the whole temperature range at the heatrun test points was covered. This allowed choosing the best matching temperature run to determine the mechanical losses for each load point.

5 | Results and Analysis

In this section, the results of the verification procedure outlined in the previous section are discussed. Each of the motor loss components is presented for all 16 test points with both the converter supply and the sinusoidal supply.

The fundamental stator Joule losses $P_{s,1}$ determined using Equation (10) with different torque levels and supply frequencies are presented in Figure 5 with both the sinusoidal supply and the converter supply. As can be seen, the stator Joule losses are clearly dependent on the torque level of the motor. The higher the torque, the higher the current and the higher the stator Joule losses. The difference in losses between the sinusoidal supply and the converter supply is higher with higher levels of motor torque. This is explained by the fact that the converter causes additional current in the stator, which generates additional heat and increases the

17518679, 2026, 1, Downloaded from https://ietresearch.onlinelibrary.wiley.com/doi/10.1049/elp2.70232 by Politecnico Di Torino Sist. Bibl Del Polit Di Torino, Wiley Online Library on [12/11/2026]. See the Terms and Conditions (https://onlinelibrary.wiley.com/terms-and-conditions) on Wiley Online Library for rules of use; OA articles are governed by the applicable Creative Commons License

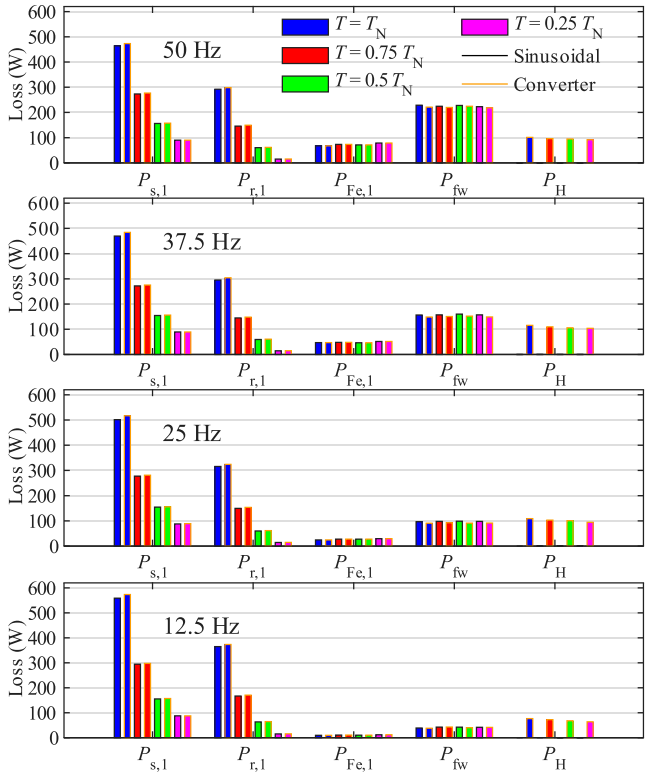


FIGURE 5 | Experimentally determined joule, iron, and friction and windage losses, and harmonic power of the motor with different load levels and different supply frequencies. Losses are presented with both sinusoidal and converter supply.

winding temperature. The higher temperature with the converter supply has an effect on the resistance of the stator, which then causes the higher $P_{s,1}$.

The fundamental rotor Joule losses $P_{r,1}$ determined using Equation (11) with different supply frequencies and load levels are presented in Figure 5 with both the sinusoidal supply and the converter supply. The Joule losses in the rotor behave in a fashion similar to the Joule losses in the stator, which, in practice, means that the Joule losses are mostly dependent on the output torque level of the motor. This, of course, is due to the fact that the current in the rotor is induced by the effect of electromotive force, which is induced by the rotating magnetic field caused by the stator currents. These are the very same currents that cause the Joule losses in the stator. As the stator resistance is higher, the air-gap voltage and flux linkage are lower, and therefore, the rotor current with the converter supply is higher, which causes the slightly higher $P_{r,1}$.

The fundamental iron losses $P_{Fe,1}$ determined using Equation (12) with different supply frequencies are presented in Figure 5. It can be clearly seen that the behaviour of the iron losses is completely different from the Joule losses. The iron losses increase as the supply frequency increases, and therefore, the rotational speed of the motor increases. Here, the fundamental iron loss values are not dependent on load as the drop in the stator resistance voltage is not taken into account. However, the torque level would have only a minor effect on the resistive voltage drop. This would require determining $P_{Fe,1}$ as a function of voltage, but this is not possible with only one no-load point. However, the effect on the iron losses would be very similar with both the converter and sinusoidal supplies, and therefore, this is not crucial for the verification purposes. The $P_{Fe,1}$ values are slightly lower with the converter supply.

Below the field-weakening operation, the motor flux is kept constant. However, due to the increased frequency, the stator iron losses are slightly increased. According to the Bertotti model, hysteresis losses are directly proportional to the supply frequency f, the eddy current losses are proportional to f^2, and the excess losses are proportional to $f^{3/2}$ [34]. Furthermore, the eddy current losses at the surface of the rotor—caused by winding harmonics [35] and air gap flux pulsations due to stator and rotor slotting—are directly proportional to the rotational speed of the rotor [36]. Therefore, an increase in the motor rotational speed increases iron losses in both the stator and the rotor. It is also important to note that the increased losses in the rotor are not affected by the time harmonics of the supply; the losses remain the same for both supply methods.

As it is presented in ref. [37], the amount of iron losses is affected by the stator and rotor core materials used with both the sinusoidal supply and the converter supply, as well as with the switching frequency [38]. The behaviour of the iron losses with both the converter supply and the sinusoidal supply in general, and a FE method for the computation of iron losses has been proposed with measurement results to verify the method, have been discussed in more detail in ref. [39].

The friction and windage losses P_{fw} with different supply frequencies are presented in Figure 5 as determined with the retardation test. The test was carried out at multiple different temperatures, and thus, for every operating point, the loss result could be chosen from the loss curve determined at the closest temperature. The results presented in Figure 5 suggest that P_{fw} are heavily dependent on the supply frequency. The reason for this is that the friction losses are higher on the bearings at higher rotational speeds and especially as the windage losses increase exponentially with speed.

The total values of the motor input high-frequency harmonic power P_H are presented in Figure 5 as determined with Equation (9). With the sinusoidal supply, the total P_H was less than 1 W at all operating points, and thus, all the sinusoidal supply bars overlap at the 0 W line in the figure. With the converter supply, the high-frequency harmonic power is significant and is obviously mostly caused by the PWM supply. P_H depends on the load according to Figure 5, but in ref. [40], it is stated that there can be a difference in some harmonic components with different loads due to the change of impedance of the motor. A more significant dependence than this is clearly observed at the supply frequency. The harmonic power is higher with the 25 and 37.5 Hz supply frequencies than with 50 Hz, which is the rated supply frequency of the motor as presented in Table 1. The behaviour of the HFH power is similar to the results presented in ref. [22].

For a more detailed inspection, the converter supply P_H is illustrated as cumulative sums of the frequency domain values obtained with Equation (2) in Figure 6. There is a load

17518679, 2026, 1, Downloaded from https://ietresearch.onlinelibrary.wiley.com/doi/10.1049/elp2.70232 by Politecnico Di Torino Sist. Bibl Del Polit Di Torino, Wiley Online Library on [12/11/2026]. See the Terms and Conditions (https://onlinelibrary.wiley.com/terms-and-conditions) on Wiley Online Library for rules of use; OA articles are governed by the applicable Creative Commons License

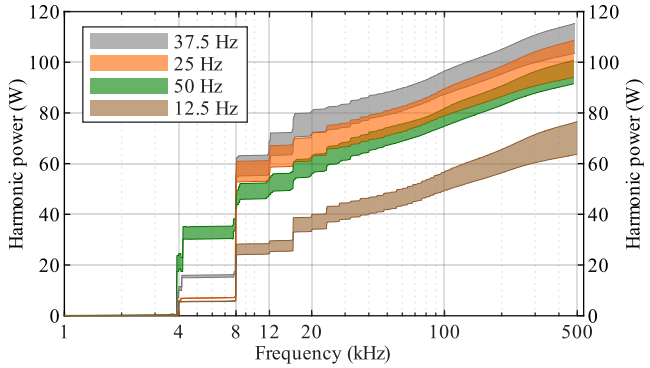


FIGURE 6 | Illustration of cumulative high-frequency harmonic power as a function of frequency with the converter supply. As the curves are cumulative and the total power is the sum of all the frequency components, the final value at the frequency of 500 kHz for each curve illustrates the total harmonic power, presented in Figure 5. Most of the harmonic power is at the switching frequency and its multiples. The differences between the load levels are small, but the harmonic powers are consistently higher with higher loads, as can be seen in Figure 5. So, curves with highest and lowest load levels measured at are presented with all the supply frequencies and coloured area between them contains the load levels between them.

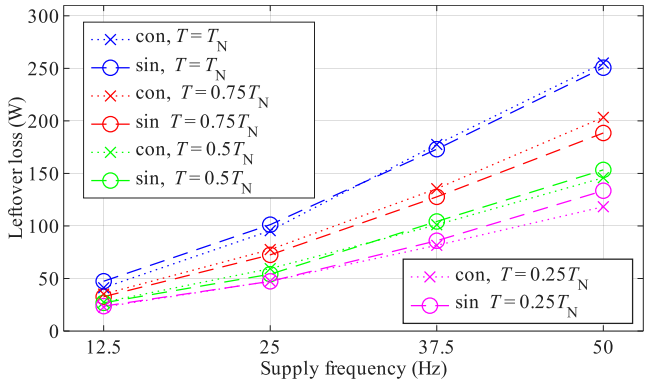


FIGURE 7 | Analytically determined leftover losses of the motor with different load levels as a function of supply frequency, while assuming that the additional harmonic losses are equal to the harmonic power. The results suggest that the leftover losses are nearly identical between supply types at all the 16 operating points in which they were determined, even if the harmonic power was very minor with sinusoidal supply, as can be seen in Figure 5. In the legend, 'sin' refers to the sinusoidal supply and 'con' to the converter supply.

dependence on the harmonic power, which is the most evident in the curve at twice the switching frequency—or the carrier frequency, as they are the same here. As seen in Figure 5, the higher the load, the higher the harmonic power within the same supply frequency. Thus, in Figure 6, the curves with load level of 100% and 25% of rated are presented as the limits of the area with one supply frequency, and load levels 75% and 50% of rated would be in that area between them. The harmonic power is highest with the supply frequency of 37.5 Hz and lowest with 12.5 Hz.

Finally, the leftover loss component P_{Lo} determined with Equation (14) is presented in Figure 7 as a function of supply frequency. It can be clearly seen that P_{Lo} depends on both the supply frequency and the load level of the motor. The measurement results presented in ref. [41] suggest the same kind of behaviour for the residual losses, as we can see here for the leftover losses. In the case of the sinusoidal supply, this is obvious as P_H is negligible (Figure 5), and can thus be omitted, reducing Equation (14) to the form of the standard residual loss equation when there is no harmonic power. Furthermore, the differences between the converter supply and the sinusoidal supply in Figure 7 are small. The differences between P_{Lo} values being small is important, because of the fact that P_{Lo} are determined as the remainder of the other loss components and P_H. This means that if some of the other loss components are inaccurate or vary between supply types, then it has an effect on P_{Lo}. The uncertainty of P_{Lo} determined in this way depends on the uncertainties of the other loss components, which is discussed in more detail in [42]. A small difference in P_{Lo} between the converter supply and the sinusoidal supply suggests that as a whole, the differences between the sinusoidal supply and the converter supply are not significant when considering only the fundamental wave frequency of the converter supply. To conclude, this indicates that the proposed method is valid and the HFH losses can be determined according to Equation (9) as

$$P_{HFH} = P_H. \tag{16}$$

6 | Discussion

Methods that are presently widely used to determine additional losses with the converter supply in comparison with the sinusoidal supply do not take into account the possible difference in the input power at the frequency of the fundamental waveform. The proposed method makes these differences visible, as can be seen in Figure 2. The additional benefit of the method is that it makes it unnecessary to run standardised comparison tests with the sinusoidal supply, and instead, the motor can be run with the converter supply only.

7 | Conclusion

The experimental results of this paper provide a basis to identify and analyse HFH losses. Although the results are shown only with a single 15 kW motor, the significance of the results should not be underestimated. The method shown here is in principle expected to be applicable to converter-driven induction motors in general, and is available for all researchers and engineers in the field. The method does not require any special tools or licences. In general, it shows that the difference between the total power and the fundamental wave power is caused by HFH losses in the motor. This opens new opportunities to analyse modulation methods, adjust the switching frequency and optimise the motor construction for the PWM supply.

The comparison of the results of the measurements suggests that the different loss components of the motor in the measured operating range do not differ significantly between runs of motor with the sinusoidal supply and the converter supply when only the fundamental wave frequency is considered with the losses of a converter-fed motor. Even the leftover loss, which is comparable to the residual loss in the case of a DOL motor, acts in a very similar manner at all the measurement points.

17518679, 2026, 1, Downloaded from https://ietresearch.onlinelibrary.wiley.com/doi/10.1049/elp2.70232 by Politecnico Di Torino Sist. Bibl Del Polit Di Torino, Wiley Online Library on [12/11/2026]. See the Terms and Conditions (https://onlinelibrary.wiley.com/terms-and-conditions) on Wiley Online Library for rules of use; OA articles are governed by the applicable Creative Commons License

One of the challenges of this comparison is to make the output powers of the motors to match between measurements. If there is a difference between the output powers, it also shows as a difference in the losses. This effect is particularly pronounced for values of leftover loss. Even when making a comparison with the same motor, the output power may be different between runs, for instance, with one being with the grid supply and another with the converter supply.

Author Contributions

Matias Tiihonen: formal analysis, software, visualization, writing – original draft. **Shoaib Ahmed:** writing – review and editing. **Hannu Kärkkäinen:** methodology, software, supervision, writing – original draft. **Markku Niemelä:** supervision, writing – review and editing. **Lassi Aarniovuori:** conceptualization, methodology, supervision, validation, writing – review and editing. **Janne Nerg:** supervision, writing – original draft. **Dong Liu:** writing – review and editing. **Aldo Boglietti:** writing – review and editing. **Radu Bojoi:** writing – review and editing.

Acknowledgements

The authors have nothing to report.

Funding

The authors have nothing to report.

Conflicts of Interest

The authors declare no conflicts of interest.

Data Availability Statement

The data that support the findings of this study are available from the corresponding author upon reasonable request.

References

1. P. Waide and C. U. Brunner, *Energy Efficiency Policy Opportunities for Electric Motor-Driven Systems* (International Energy Agency (IEA), 2011).

2. IEA, *Global EV Outlook 2024 Moving Towards Increased Affordability* (International Energy Agency (IEA), 2024).

3. A. Veltman, D. W. J. Pulle, and R. W. De Doncker, *Fundamentals of Electrical Drives, Power Systems* (Springer International Publishing, 2016).

4. IEEE, "IEEE Standard Test Procedure for Polyphase Induction Motors and Generators," IEEE Std 112-2017 (Revision of IEEE Std 112-2004) (2018), 1–115.

5. International Electrotechnical Commission, "Rotating Electrical Machines—Part 2-1: Standard Methods for Determining Losses and Efficiency From Tests (Excluding Machines for Traction Vehicles)," IEC 60034-2-1 (June 2014).

6. International Electrotechnical Commission, "Rotating Electrical Machines—Part 2-3: Specific Test Methods for Determining Losses and Efficiency of Converter-Fed AC Motors," IEC 60034-2-3 (March 2024).

7. A. Boglietti, A. Cavagnino, M. Cossale, A. Tenconi, and S. Vaschetto, "Efficiency Determination of Converter-Fed Induction Motors: Waiting for the IEC 60034-2-3 Standard," in *2013 IEEE Energy Conversion Congress and Exposition* (2013), 230–237.

8. International Electrotechnical Commission, "Rotating Electrical Machines—Part 30-1: Efficiency Classes of Line Operated AC Motors (IE Code)," IEC 60034-30-1 (March 2014).

9. International Electrotechnical Commission, "Rotating Electrical Machines—Part 30-2: Efficiency Classes of Variable Speed AC Motors (IE-code)," IEC TS 60034-30-2 (December 2016).

10. T. Marvin Undeland and N. Mohan, "Overmodulation and Loss Considerations in High-Frequency Modulated Transistorized Induction Motor Drives," *IEEE Transactions on Power Electronics* 3, no. 4 (1988): 447–452, https://doi.org/10.1109/63.17966.

11. K. Yamazaki and S. Kuramochi, "Additional Harmonic Losses of Induction Motors by PWM Inverters: Comparison Between Result of Finite Element Method and IEC/TS 60034," in *2012 XXth International Conference on Electrical Machines* (2012), 1552–1558.

12. International Electrotechnical Commission, "Rotating Electrical Machines—Part 25: AC Electrical Machines Used in Power Drive Systems—Application Guide," IEC TS 60034-25 (June 2022).

13. H. Kärkkäinen, P. Lindh, L. Aarniovuori, M. Tiihonen, and N. Markku, "Loadability of Converter-Fed Induction Machine," in *2023 25th European Conference on Power Electronics and Applications (EPE'23 ECCE Europe)* (2023), 1–8.

14. A. Tessarolo and F. Luise, "A Finite Element Approach to Harmonic Core Loss Prediction in VSI-Fed Induction Motor Drives," in *2008 International Symposium on Power Electronics, Electrical Drives, Automation and Motion* (2008), 1309–1314.

15. S. Lee and J. Yun, "Influence of Electrical Steel Characteristics on Efficiency of Industrial Induction Motors," in *2017 20th International Conference on Electrical Machines and Systems (ICEMS)* (2017), 1–4.

16. L. Jeong-Jong, Y.-K. Kim, H. Nam, K.-Ho Ha, J.-P. Hong, and D.-Ha Hwang, "Loss Distribution of Three-Phase Induction Motor Fed by Pulsewidth-Modulated Inverter," *IEEE Transactions on Magnetics* 40, no. 2 (2004): 762–765, https://doi.org/10.1109/TMAG.2004.825445.

17. X. Fan, D. Li, W. Kong, L. Cao, R. Qu, and Z. Yin, "Fast Calculation of Strand Eddy Current Loss in Inverter-Fed Electrical Machines," *IEEE Transactions on Industrial Electronics* 70, no. 5 (2023): 4640–4650, https://doi.org/10.1109/tie.2022.3183338.

18. Y. Zhan, B. Li, H. Zhao, G. Xu, and D. Zhang, "Fast Solution of Rotor Losses in Inverter-Fed Cage Induction Motors With Skewed Slots," *IEEE Transactions on Industry Applications* 56, no. 2 (2020): 1284–1292, https://doi.org/10.1109/tia.2019.2957970.

19. D. Zhang, J. Yi, H. Zhu, et al., "The Electromagnetic Losses Analysis of Inverter-Fed Induction Motor Accounting for Interbar Current and Rotor Slip Frequency," *IEEE Transactions on Transportation Electrification* 8, no. 1 (2022): 1155–1167, https://doi.org/10.1109/tte.2021.3104400.

20. A. Fatima, R. Kumar, Ze Li, G. Byczynski, and N. C. Kar, "An Accurate Core Loss Model of Inverter-Fed Induction Machine Considering Supply and Saturation Harmonics," *IEEE Transactions on Transportation Electrification* 11, no. 4 (2025): 10402–10414, https://doi.org/10.1109/TTE.2025.3551602.

21. C. Mathews, J. Mushenya, M. A. Khan, and S. B. Paul, "Non-Intrusive Efficiency Estimation of Inverter-Fed Induction Motors," *IEEE Transactions on Energy Conversion* 38, no. 3 (2023): 1845–1854, https://doi.org/10.1109/TEC.2023.3242173.

22. L. Aarniovuori, H. Kärkkäinen, M. Niemelä, and J. Pyrhönen, "PWM-Induced Harmonic Power in 75 kW IM Drive System," in *2020 22nd European Conference on Power Electronics and Applications (EPE'20 ECCE Europe)* (2020), 1–9.

23. A. Anttila, L. Aarniovuori, M. Niemelä, M. Zaheer, P. Lindh, and P. Juha, "Active Power Analysis of PWM-Driven Induction Motor in

17518679, 2026, 1, Downloaded from https://ietresearch.onlinelibrary.wiley.com/doi/10.1049/elp2.70232 by Politecnico Di Torino Sist. Bibl Del Polit Di Torino, Wiley Online Library on [12/11/2026]. See the Terms and Conditions (https://onlinelibrary.wiley.com/terms-and-conditions) on Wiley Online Library for rules of use; OA articles are governed by the applicable Creative Commons License

Frequency Domain," in *2021 XVIII International Scientific Technical Conference Alternating Current Electric Drives (ACED)* (2021), 1–6.

24. H. Kärkkäinen, L. Aarniovuori, S. Makkonen, M. Niemelä, and P. Juha, "Determination of High-Frequency Harmonic Power in Converter-Fed Motors," in *2022 International Conference on Electrical Machines (ICEM)* (2022), 394–400.

25. L. Aarniovuori, M. Tiihonen, S. Ahmed, et al., "Segregation of Additional High Frequency Harmonic Losses Created by PWM Supply," in *2024 IEEE 65th International Scientific Conference on Power and Electrical Engineering of Riga Technical University (RTUCON)* (2024), 1–6.

26. I. Takahashi and H. Mochikawa, "A New Control of PWM Inverter Waveform for Minimum Loss Operation of an Induction Motor Drive," *IEEE Transactions on Industry Applications IA-* 21, no. 3 (1985): 580–587, https://doi.org/10.1109/tia.1985.349713.

27. International Electrotechnical Commission, "Rotating Electrical Machines—Part 2-3: Specific Test Methods for Determining Losses and Efficiency of Converter-Fed AC Induction Motors," IEC TS 60034-2-3 (November 2013).

28. IEEE, "IEEE Standard Definitions for the Measurement of Electric Power Quantities Under Sinusoidal, Nonsinusoidal, Balanced, or Unbalanced Conditions," IEEE Std 1459-2010 (Revision of IEEE Std 1459-2000) (2010): 1–50.

29. S. Smith, *Digital Signal Processing: A Practical Guide for Engineers and Scientists, Demystifying Technology Series* (Elsevier Science & Technology, 2002)

30. C. Elwood Shannon, "Communication in the Presence of Noise," *Proceedings of the IRE* 37, no. 1 (1949): 10–21, https://doi.org/10.1109/jrproc.1949.232969.

31. International Electrotechnical Commission, "Rotating Electrical Machines—Part 2-2: Specific Methods for Determining Separate Losses of Large Machines From Tests—Supplement to IEC 60034-2-1," IEC 60034-2-2 (March 2024).

32. Yokogawa Test & Measurement Corporation, "Where Power Meets Precision: PX8000 Precision Power Scope," (May 2023) [Online], https://cdn.tmi.yokogawa.com/1/2677/files/BUPX8000-01EN.pdf.

33. H. Kärkkäinen, L. Aarniovuori, M. Niemelä, and P. Juha, "Advanced Uncertainty Calculation Method for Converter-Fed Motor Loss Determining," in *2019 IEEE International Electric Machines & Drives Conference (IEMDC)* (2019), 1551–1558.

34. Giorgio Bertotti, "General Properties of Power Losses in Soft Ferromagnetic Materials," *IEEE Transactions on Magnetics* 24, no. 1 (1988): 621–630, https://doi.org/10.1109/20.43994.

35. R. Richter, *Elektrische Maschinen. Band IV die Induktionsmaschinen* (Verlag Birkhäuser, 1954).

36. B. Heller and V. Hamata, *Harmonic Field Effects in Induction Machines* (Elsevier Scientific Pub. Co, 1977).

37. M. Dems and K. Komeza, "The Influence of Electrical Sheet on the Core Losses at No-Load and Full-Load of Small Power Induction Motors," *IEEE Transactions on Industrial Electronics* 64, no. 3 (2017): 2433–2442, https://doi.org/10.1109/tie.2016.2587817.

38. L. Danilo Tornello, S. Vaschetto, E. B. Agamloh, G. Scelba, G. De Donato, and A. Cavagnino, "Investigating PWM-Induced Iron Losses: Measurements and Estimation Models Up to 350 kHz Switching Frequency," *IEEE Open Journal of Industry Applications* 5 (2024): 338–355, https://doi.org/10.1109/ojia.2024.3430861.

39. Z. Gmyrek, A. Boglietti, and A. Cavagnino, "Estimation of Iron Losses in Induction Motors: Calculation Method, Results, and Analysis," *IEEE Transactions on Industrial Electronics* 57, no. 1 (2010): 161–171, https://doi.org/10.1109/tie.2009.2024095.

40. W. Cao, K. J. Bradley, J. C. Clare, and P. W. Wheeler, "Comparison of Stray Load and Inverter-Induced Harmonic Losses in Induction Motors Using Calorimetric and Harmonic Injection Methods," *IEEE Transactions on Industry Applications* 46, no. 1 (2010): 249–255, https://doi.org/10.1109/tia.2009.2036675.

41. R. Kumar, B. Sah, and P. Kumar, "Stray Loss Formulation for Inverter-Driven Induction Motors for a Wide Range of Switching Frequency and Motor's Loading," *IEEE Transactions on Industrial Electronics* 71, no. 3 (2024): 2385–2394, https://doi.org/10.1109/tie.2023.3269484.

42. G. Bucci, F. Ciancetta, E. Fiorucci, S. Mari, and M. A. Segreto, "The Measurement of Additional Losses in Induction Motors: Discussion About the Actually Achievable Uncertainty," *Energies* 13, no. 1 (2019): 78, https://doi.org/10.3390/en13010078.

17518679, 2026, 1, Downloaded from https://ietresearch.onlinelibrary.wiley.com/doi/10.1049/elp2.70232 by Politecnico Di Torino Sist. Bibl Del Polit Di Torino, Wiley Online Library on [12/11/2026]. See the Terms and Conditions (https://onlinelibrary.wiley.com/terms-and-conditions) on Wiley Online Library for rules of use; OA articles are governed by the applicable Creative Commons License